Experiment of Digital Directional Modulation Transmitters

Yuan Ding and Vincent F. Fusco
The Institute of Electronics, Communications and Information Technology (ECIT), Queen's University Belfast, Belfast, United Kingdom, BT3 9DT
(Email: yding03@qub.ac.uk; v.fusco@qub.ac.uk)

***Abstract*—A digital directional modulation (DM) transmitter structure is proposed from a practical implementation point of view in this paper. This digital DM architecture is built with the help of several off-the-shelf physical layer wireless experiment platform hardware boards. When compared with previous analogue DM transmitter architectures, the digital means offers more precise and fast control on the updates of the array excitations. More importantly, it is an ideal physical arrangement to implement the most universal DM synthesis algorithm, i.e., the orthogonal vector approach. The practical issues in digital DM system calibrations are described and solved. The bit error rates (BERs) are measured via real-time data transmissions to illustrate the DM advantages, in terms of secrecy performance, over conventional non-DM beam-steering transmitters.**

***Index Terms*— Bit error rate (BER), digital directional modulation (DM), orthogonal vector, security.**

I. INTRODUCTION

Directional modulation (DM) concept [1]–[6] was proposed to enable secure wireless communication in free space directly at the physical layer, in such a fashion information theoretical security [7] could be obtained, beyond what could be achieved by classical cryptographic technologies [8].

Generally speaking, DM is a transmitter side technology that is capable of projecting digitally-encoded information signals into a pre-specified spatial direction in free space while simultaneously distorting the constellation formats of the same signals along all other directions. This definition was first mathematically described in [9], [10] via an established vector model.

In the recent extensive DM research works [1]-[6], [9]-[25], the physical arrangements that enable DM functionalities can be sorted into four categories. The first is the parasitic DM architecture, termed near-field direct antenna modulation (NFDAM) by authors in [1]-[3]. This type of DM transmitter consists of a large number of parasitic antenna structures with switches embedded, and placed in the near-field of a central driven antenna element. The large aperture electric size makes this DM structure less attractive for microwave applications. Furthermore, complex interaction between near-field electro-magnetic boundaries and far-field transformations makes trial-and-error the only synthesis method that can be applied. The second type of DM structures, named as active DM architecture, comprises of antenna arrays, in which each antenna element is actively excited by radio frequency (RF) carriers whose phases and/or magnitude can be altered by baseband information data controlled RF-reconfigurable components. Most DM researches, e.g., [4], [6], [11]-[17] adopted this structure since an analytical link between the antenna array excitations or component settings, and the far-field radiation behavior facilitates the development of effective and efficient DM synthesis approaches, e.g., [4], [10], [16]-[19]. Another type of DM transmitters employs beam-forming networks, which can be switch arrays [20]-[23] or Fourier lenses [24], [25], before the antenna array. Since the employed beam-forming networks can be regarded as hardware realizations of DM synthesis algorithms, the additional DM array excitation syntheses are not required for this type of DM structure. The last, but the most powerful and practical, from the implementation point of view, DM transmitter solution is the digital DM structure presented in [9], [10]. This promising digital DM architecture utilizes mature digital baseband modules, onto which DM algorithms are applied. Compared with above mentioned three other types of DM structures, the digital DM transmitters have the following advantages;

- No reconfigurable RF components, e.g., switches [1]-[3], [5], [20]-[23], phase shifters [4], [6], [11]-[17], and attenuators [16], [17], which are often associated with bulky bias and control units and need to operate at a speed much higher than the information data rates, are required for digital DM transmitters.
- The antenna array excitations can be more precisely controlled by digital means other than by analogue RF components, e.g., a commonly used 12-bit digital-to-analogue converter (DAC) can synthesize a continuous wave with phase resolution less than 0.1°, which is equivalent to that of a 12-bit RF phase shifter that is not commercially available.
- No RF insertion loss is introduced in digital DM transmitters. For other DM structure types, the insertion loss of RF component means power amplifiers (PAs) with higher output power are required, which not only increase the system cost but also decrease the system power efficiency.

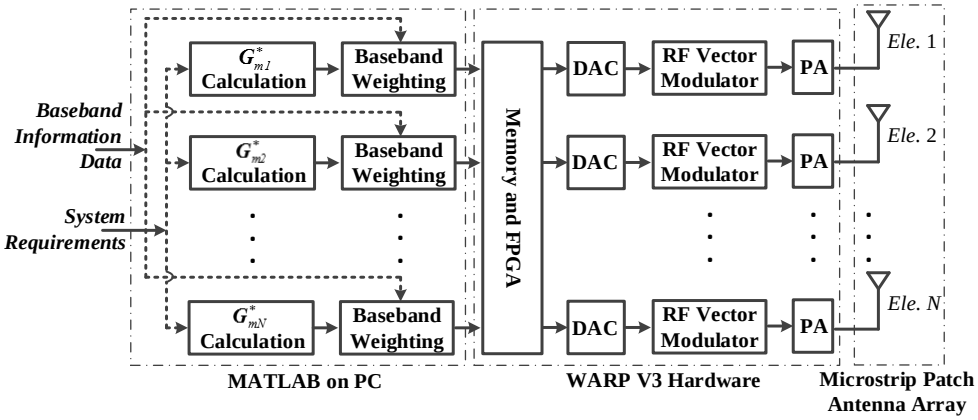

Fig. 1. Digital DM transmitter architecture.

- Since in the digital DM transmitters the DM algorithms are applied at the digital baseband, the classical data coding and cryptographic technologies can be readily appended in a straightforward manner.
- System calibrations for the digital DM structures can be conducted without disassembling the transmitters, while for the others the antenna arrays, RF cables, and the employed RF components have to be calibrated separately. This system calibration aspect will be elaborated in Section IV.
- The digital DM structure is compatible with any DM synthesis approaches. It should be noted that the fact previously mentioned that the DM structures in [20]–[25] do not require array excitation synthesis. On the other hand, this also indicates the impossibility of changing DM algorithms which can focus on different DM performance characteristics, e.g., bit error rate (BER) performance [16], [17] and array far-field radiation patterns [18], [19].

This paper is devoted to the investigation of the digital DM architecture, particularly on its physical implementation and experimental validation. The paper is organized into 6 sections. Section I as already presented provided readers an overview of the DM technology, especially on its physical structures available. The advantages of the digital DM structure, compared with the analogue ones, were summarized. In Section II the digital DM architecture is presented from a practical implementation point of view. Before the experimental setup is described in Section IV, a physical layer wireless experiment platform, called Wireless Open-Access Research Platform (WARP) [26], and utilized herein for digital DM experiments, is briefly introduced in Section III. Experimental results and discussion are provided in Section V. Conclusions are drawn in Section VI.

II. Digital DM Architecture

The digital DM architecture, in its generic form introduced in Fig. 1 in [10], is more powerful and flexible, when compared with the analogue DM transmitter architectures presented in [1]-[6], [11]-[17], [20]-[25], as we discussed in Section I.

In order for readers to facilitate a better understanding of the digital DM experimental setup described later in this paper, the digital DM transmitter architecture is restated here in Fig. 1 with major system blocks labelled.

It is noticed in Fig. 1 that the WARP considerably simplifies the digital DM transmitter structure implementation. Thus it is briefly introduced in the following section.

III. Introduction to the Wireless Open-Access Research Platform (WARP)

WARP is a scalable and extensible wireless platform, which, for the V3 hardware we employed, integrates a Xilinx Virtex-6 FPGA with other functional peripherals, including four programmable RF interfaces (expanded with a FMC-RC-2X245 radio module via the FMC HPC slot), user Input/Output (I/O), Memory, and Ethernet sockets, see Fig. 2.

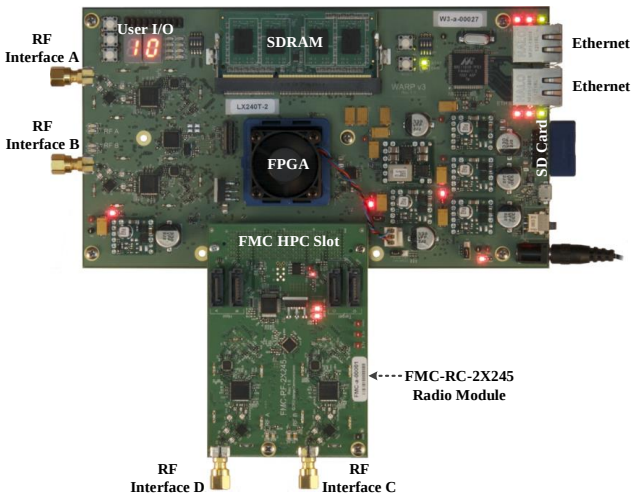

Fig. 2. WARP V3 hardware [26].

There are two different methods to prototype with WARP hardware. One is to add additional customized intellectual property (IP) cores that are executed directly by hardware circuits synthesized in FPGA. This method guarantees real-time processing but often leads to a longer development cycle. The other way is to separate digital baseband signal generation (in transmitter mode) and signal analysis (in receiver mode)

from real-time hardware operations. These baseband signal processing operations can be performed offline in MATLAB on a PC. It is noted that signals over the wireless channel are still transmitted in a real-time manner. This MATLAB-based method with a design template we used, WARPLab 7, provides us a means for rapid physical layer prototyping that allows for coordination of arbitrary combinations of single and multi-antenna transmit and receive nodes, and is also very flexible and extensible for various signal processing algorithms. This is the approach we adopt, since all of these features are core to digital DM implementation.

The WARPLab platform has a layered structure, i.e., the physical setup, the hardware and software design, and finally the algorithms implemented in MATLAB. The workflow of a typical data transmission event is now explained from the PC's point of view. Assume that WARP nodes are ready to work and can communicate to the PC via an Ethernet switch. The PC first initializes the system, including setting the port numbers and board physical addresses. This is done by looking up the MACRO defined in the header files both in the PC and WARP nodes. Then the PC sends commands to WARP nodes to set key parameters, such as operation frequency, transmit/receive gains, transmit mode, and so on. Data generation and processing (coding and modulation) is performed in MATLAB. Data is packed into a fixed-length frame, of which the length cannot exceed the size of the allocated data buffer in FPGA, i.e., 2^{+15} bits for the WARP V3 hardware. Once the data packets are downloaded into the buffer via TCP/IP protocol, the WARP nodes are ready to send and receive data. It is done automatically after a trigger is received from the PC. The receive node captures, frequency down-converts, and samples signals, and then feeds digitized samples back to the PC for analysis, which is performed in MATLAB. Normally the raw data are processed by a demodulator and decoder in order to recover the original data bits.

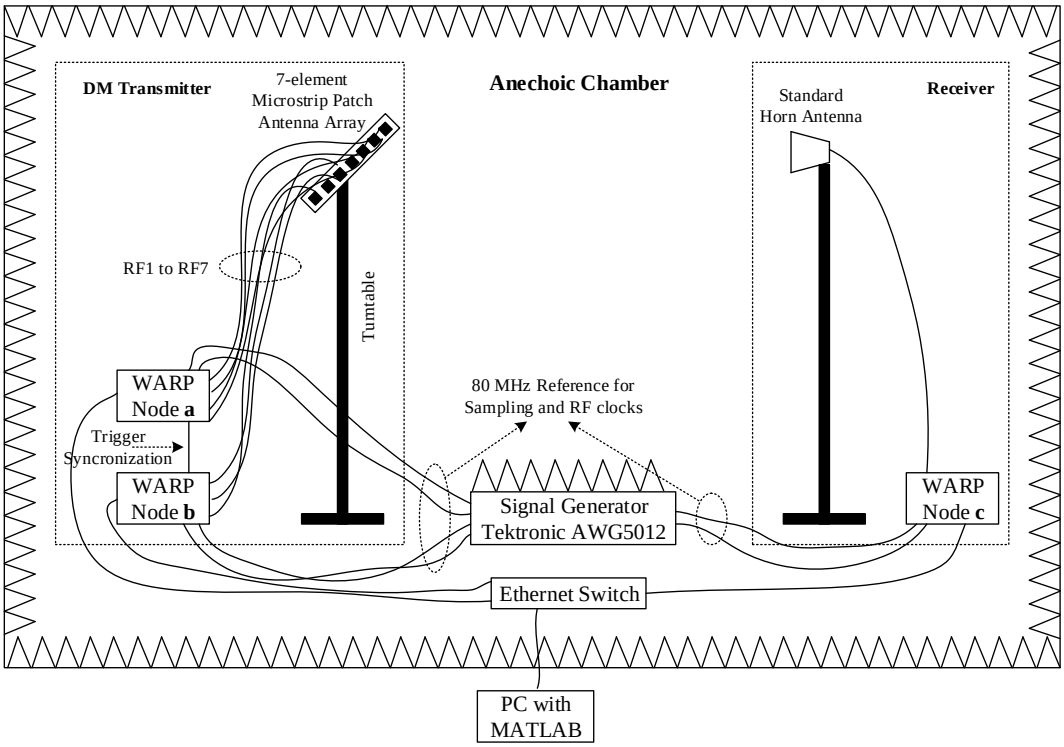

Fig. 3. Block diagram of the digital DM experimental setup.

IV. Experimental Setup

The block diagram of the digital DM experimental setup is presented in Fig. 3, and photographs are shown in Fig. 4.

The digital DM system workflow is now described in detail;

a) Initialize the WARP nodes **a**, **b**, and **c**, see Figs. 3 and 4. This includes

- identifying the physical address of each WARP board,
- allocating RF port numbers. To facilitate discussion, they are labelled as RF1 to RF8 (RF1 to RF4 on transmit node **a**, RF5 to RF7 on transmit node **b**, and RF8 on receive node **c**),
- setting operation frequency. 2.442 GHz (channel 7 in 2.4 GHz ISM band) was used in the experiment. This value was chosen to match the resonant frequency of the microstrip patch antenna array that will be presented later in this section.
- setting transmitter and receiver gains, including both baseband and RF gains. The basic rules are: choose medium and identical gain for each transmitter chain, i.e., RF1 to RF7, in order to reduce non-linearity that active devices, e.g., PA, generate; choose low gain for the receiver chain RF8 to mitigate detection of weak transmitted signals coupled directly onto the receive cables and board.

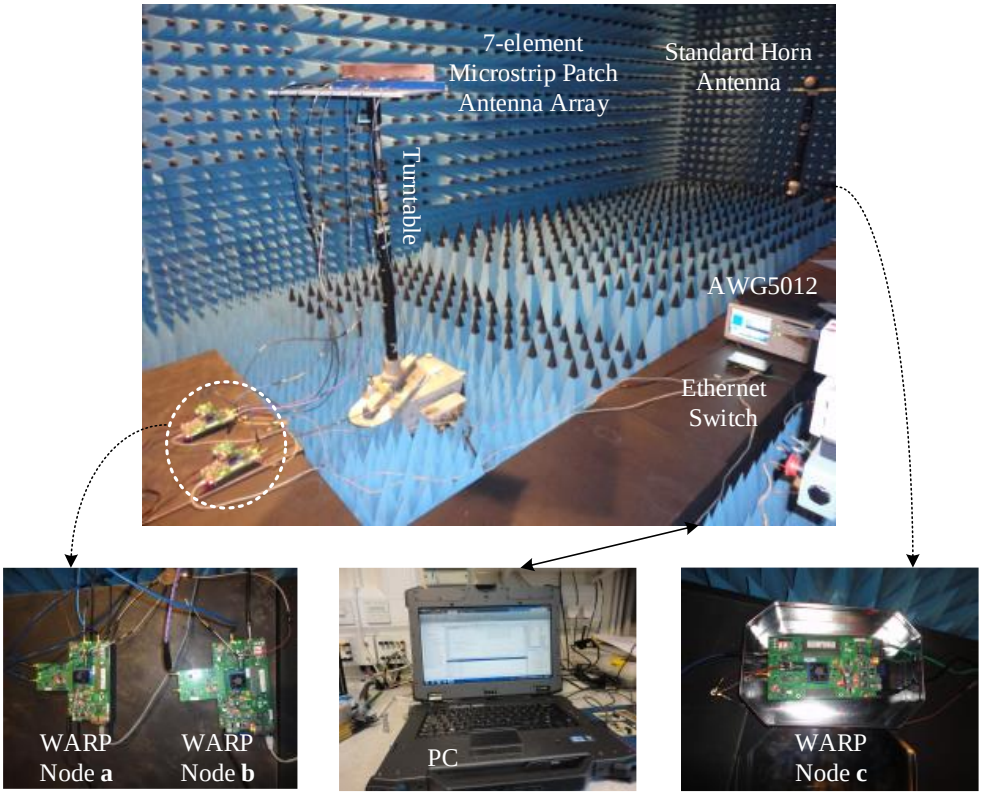

Fig. 4. Photographs of the digital DM experiment.

b) Steer the one-dimensional (1-D) transmit antenna array in azimuth to align the standard receive horn antenna along the pre-specified secure communication direction θ_0, 60° selected in the experiment presented in this paper.

c) Calibrate magnitude and synchronize phase of the radiated signal at each microstrip patch antenna element along θ_0. This step will be elaborated later in this section.

d) Download data samples, onto which the DM algorithms are applied, into the dedicated buffer for each transmit chain in the FPGAs. We adopted the universal DM synthesis approach, orthogonal vector algorithm, developed in [10] to construct the dynamic DM system in the experiment reported below. Any of the other synthesis methods, presented in [16]–[19], could equally have been used. The transmit data samples are obtained as follows;

- Generate a sequence of random data bits, which are then mapped into 2-bit symbols and modulated with Gray-coded differential QPSK (DQPSK). Differential modulation scheme is chosen because it simplifies demodulation at receive side, since initial phase value is not required. The uniform envelope of DQPSK also helps reduce unwanted system non-linearity effects.
- Append preamble that is a Barker sequence modulated with Binary Phase-Shift Keying (BPSK) ahead of the DQPSK signals obtained in the last step. This is done for identifying where the data starts in the receive buffer after signals are captured on the receive side.
- Process the preamble-appended signals with a square-root raised cosine finite impulse response (FIR) filter in order to limit the effective bandwidth of the transmission and minimize inter-symbol interference that may be caused by wireless channels with equipment presented. The filter order chosen is 16, and rolloff factor is 0.3.
- Up-convert the filtered baseband signals to a center frequency of 5 MHz in order to avoid direct current (DC) attenuation in the transceiver MAX2829 [27].
- Generate a matrix, termed the interference matrix, with each row a random orthogonal vector that satisfies the DM system requirement of power efficiency PE_{DM}, see the definition in (25) in [10]. The size of the interference matrix is (buffer length)×(N, the number of the transmitter array element) = 2^{+15}×7.
- The final data samples for the i^{th} (i = 1, 2, …, 7) transmit RF chain that are ready for downloading into the corresponding FPGA transmit buffers are obtained by summing the 5 MHz up-converted signals and the i^{th} column of the generated interference matrix.

All the above steps a) to d) are performed in MATLAB.

e) Rotate the DM transmit antenna array to align the receive horn antenna along the spatial direction θ ($\theta \in [0°, 180°]$) of interest.

f) Send triggers to the WARP nodes **a**, **b**, and **c**. When the triggers are received, the data samples in FPGA transmit buffers are pushed into DACs at the sampling frequency- 40 MHz- before being up-converted to 2.442 GHz by the transceiver MAX2829 and radiated through the patch antenna array. The transmitted signals along θ, captured by the receive horn antenna, are down-converted by the MAX2829, and digitized through an analogue-to-digital converter (ADC), and then stored in the receive buffer in

the WARP node **c**. The recovered raw data is read into MATLAB.

g) In MATLAB, add artificial AWGN onto the received raw data. This manipulation facilitates the investigation of system performance under various signal-to-noise ratio (SNR) conditions. The system inherent AWGN is sufficiently low to be ignored. This was validated through an experiment where zero BER after 10^{+6} data bits transmissions were detected along any spatial directions in a conventional non-DM system when positioned in an anechoic chamber.

h) The noisy raw data is down-converted to baseband by multiplying a 5 MHz carrier and then processing it through a matched square-root raised cosine finite impulse response (FIR) filter. By finding the maximum correlation coefficient between the up-sampled preamble Barker sequence and the filtered samples, the beginning of the real transmitted data signals in the receive buffer can be identified. These signals are then down-sampled, Differential-QPSK (DQPSK) demodulated, and decoded into a bit sequence. The number of error bits is obtained by comparing this decoded bit sequence with the generated bit sequence in the step d).

i) Iterate steps f) to h) until the required number of data bits are transmitted, 10^{+6} was used in the experiment. Excluding the transmit buffer space W (bits) used for preamble and data protection, the actual number of data bits transmitted in each f) to h) event is approximately 2000, i.e., $(2^{+15}–W)/R_{os}$. R_{os} is the oversampling rate, chosen to be 16 in the experiment. R_{os} = 16 also indicates that the symbol rate during the transmission is (sampling clock)/R_{os} = 40/16 = 2.5 Msps (Million symbols per second). In order to transmit 10^{+6} data bits, around $10^{+6}/2000$ = 50 iterations are required. With the total number of bits in error and the total number of transmitted bits known, the BER along θ can be calculated.

j) Scan θ within 0° to 180° and repeat steps f) to i). BER spatial distribution is obtained under pre-specified orthogonal vector injection power and SNR conditions.

Before presenting sample experimental results in Section V, the characteristics of the 1-D 7-element microstrip patch antenna array used in the experiment are illustrated, and the procedures for system calibration mentioned in the step c) are discussed in the remaining part of this section.

A. 1-D 7-element Microstrip Patch Antenna Array

A 1-D half wavelength spaced 7-element microstrip patch antenna array operating at 2.442 GHz to be used in the digital DM experiment was fabricated on GML1000 substrate [28], thickness 1.52 *mm* and dielectric constant 3.05, and is shown in Fig. 5. The overall array dimension is 450 *mm* × 100 *mm*. The measured S-parameters are depicted in Fig. 6. It can be seen that the resonant frequency of each antenna element in the array is virtually identical, 2.442 GHz, while the cross coupling between each two elements is kept sufficient low, below −17 dB. The weak coupling effect makes the channel

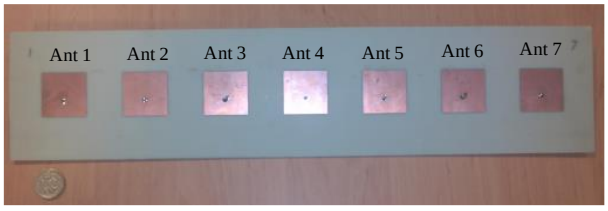

Fig. 5. Front view of the fabricated 1-D 7-element microstrip patch antenna array for 2.442 GHz operation. A ground plane covers the entire back of the board.

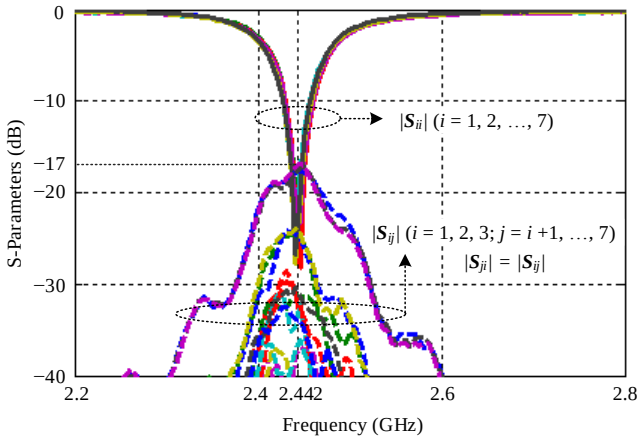

Fig. 6. Measured S-parameters of the fabricated 1-D 7-element patch antenna array.

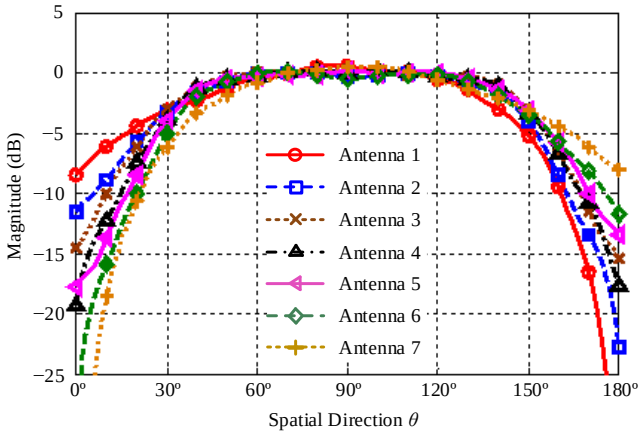

(a)

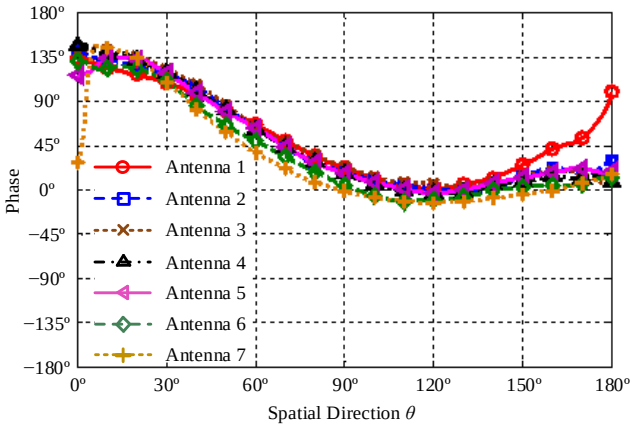

(b)

Fig. 7. Measured AEP, both (a) normalized magnitude and (b) phase, of each antenna element in the array.

vector definition in the orthogonal vector DM synthesis approach presented in [10] applicable.

The far-field active element pattern (AEP) [29], both magnitude and phase, of each antenna element with all the remaining ports 50 Ω terminated, was measured in an anechoic chamber and is presented in Fig. 7. Here we normalize the magnitude value of the center element, i.e., antenna 4, along boresight (90°) to be 0 dB. Each antenna element is estimated to have the gain of around 7 dBi. In order to facilitate a comparison, the measured phase patterns in Fig. 7 (b) have been post-processed to assure the alignment between the antenna test rotator axis and the physical geometric center of each corresponding patch antenna element.

B. System Calibration

There are several aspects that need to be calibrated before the proposed digital DM experimental system becomes operational. These are now addressed;

a) Sampling clock and RF interface clock frequency synchronization:

This is a core critical aspect for the successful implementation of the digital DM architecture. The sampling clock, 40 MHz, which is obtained by dividing the sampling reference clock of 80 MHz by 2, is used, for transmit nodes, to push data stored in the transmit buffers serially out into DACs, while for receive nodes, to sample received analogue signals by ADCs after frequency down-conversion. The 80 MHz sampling reference clock can be provided by an on-board temperature-compensated crystal oscillator (TCXO) or an external source via the clock module CM-MMCX.

Similarly the RF interface clock, 40 MHz, which is obtained by dividing the RF reference clock of 80 MHz by 2, is used for generating the 2.442 GHz RF carriers, for transmit nodes, up-conversion, and for receive nodes, down-conversion. The 80 MHz RF reference clock can be provided by an on-board TCXO or an external source via the clock module CM-MMCX.

Unsynchronized sampling clock and RF interface clock frequencies between transmit and receive nodes can significantly distort received data, especially since the RF interface clock frequencies are scaled up by more than 50 times to synthesize the RF carriers. The sensitivity of clock frequency makes the use of separate on-board TCXOs unfeasible. There are two ways to solve this issue. One is to route the TCXO output on one board to all other boards. However this direct cable connection between transmit and receive nodes creates an un-ignorable data link due to cross-coupling effects which could ruin the experiment. The other method, the one we adopted in the experiment, is to use an external stable frequency reference, a Tektronic AWG5012 [30], to generate required sampling and RF reference clocks for every WARP nodes. The equipment also provides excellent isolation between transmit and receive nodes.

b) Trigger synchronization:

A WARP board begins to transmit or receive when a trigger signal is detected. In order to make 7 transmit data chains, which are located in two WARP nodes, be activated simultaneously, trigger synchronization between two transmit boards was enabled.

c) Calibration of the far-field radiation patterns of the transmit antenna array:

It can be seen in Fig. 7 that the magnitude and phase in each antenna radiation pattern along the selected secure communication direction θ_0, i.e., 60°, are not identical. To deal with this issue we can either modify the channel vector used for orthogonal vector generation or make calibration by individually weighting the transmitted signal that is radiated through each corresponding antenna element. The calibration method, which we chose for the experiment, can be achieved together with the WARP transmit node gain and phase calibrations that will be investigated in the following steps d) and e). This combination approach simplifies the entire calibration process and minimizes errors.

d) Gain calibration of each transmit RF chain, RF1 to RF7:

Although the power gain in each transmit chain is set to be identical, the magnitudes of RF outputs, when the same baseband signal is transmitted, for different ports can differ by around 1 dB due to chipsets and cable loss differences. We calibrate the RF gain and the antenna radiation gain simultaneously following the below procedure;

- Rotate the transmit antenna array in azimuth in the anechoic chamber in order to align the receive antenna along the selected communication direction θ_0.
- Generate a fixed random bit stream which is then modulated with DQPSK.
- Append a preamble Barker sequence, modulated with BPSK.
- Individually transmit this baseband signal via each RF chain. The average magnitudes U_i (i = 1, 2, …, 7) of the received DQPSK symbols can be exploited for gain calibration by weighting each baseband signal with corresponding C/U_i. C is a constant adjusted to make use of the full range of the DACs at the transmit side.
- Re-transmit the C/U_i scaled baseband signal via each corresponding RF chain, and detect the average magnitudes V_i (i = 1, 2, …, 7) of the received DQPSK symbols. Thus the overall calibration coefficients applied at baseband signals for RF gain and antenna radiation gain calibration are obtained as $C/(U_iV_i)$. The scaling procedure is performed twice to minimize the effect that circuit non-linearity may introduce.

We verified the gain calibration coefficients $C/(U_iV_i)$ by transmitting the coefficients weighted baseband signal via each RF chain. It was found that the output power differences were less than 0.08 dB.

e) Phase synchronization of each transmit RF chain, RF1 to RF7:

The RF carriers with frequency of 2.442 GHz used for up-conversion in each transmit RF chain have been

frequency synchronized by providing a common external RF reference clock. However, the phase relations among 7 RF carriers can be arbitrary, but they are fixed with respect to time after each RF chain is powered up. These RF carrier phase differences, together with the phase differences introduced by the non-identical antenna radiation phase patterns and different lengths of coaxial cables between the WARP transmit RF ports and the antenna array are eliminated following the steps below;

- Similar to the gain calibration, rotate the transmit antenna array in azimuth in the anechoic chamber to align the receive antenna along the selected communication direction θ_0.
- Transmit a non-modulated RF carrier $C/(U_1V_1)\cdot sin(2\pi f_c t)$ via the RF1 and the Antenna 1, while simultaneously and alternately radiating $C/(U_iV_i)\cdot sin(2\pi f_c t+\varphi_i+2\pi s/S)$ through the i^{th} RF chain and the i^{th} antenna element (i = 2, 3, …, 7). f_c is the carrier frequency, 2.442 GHz. S is the sample length of the data payloads which we chose to be 2^{+14}. This indicates that the phase resolution is $2\pi\times2^{-14}$. s is sample number index, increasing from 0 to $2^{+14}-1$. By identifying sample indexes s_i that correspond to the minimum power of received signals, the phase differences φ_i between the i^{th} and the 1st paths can be computed by $\pi-2\pi s_i/S$.
- Finally, the obtained φ_i can be added into the 5 MHz up-conversion step in baseband to achieve phase synchronization among all 7 transmit chains. It is noted that in practice, a preamble is appended before the carrier signal in RF1 in order to eliminate the trigger difference between transmit nodes and receive node.

Apart from phase differences caused by RF carriers, antenna phase responses, and coaxial cables between the WARP transmit nodes and the antenna array, the above phase synchronization procedures also cancel out the phase displacements caused by the different lengths of wireless propagation paths between the i^{th} transmit antenna and the receive antenna, i.e., $(i-1)\pi cos(\theta_0)$. As a consequence the channel vector $\bar{\boldsymbol{H}}_{ov}$ used in the orthogonal vector DM synthesis approach for the experiment becomes $[1\ 1\ 1\ 1\ 1\ 1\ 1]^T$. '$[\cdot]^T$' denotes the vector transpose operator.

V. Experimental Results and Discussion

Following the experimental procedures described in Section IV, the experimental BER results obtained for the 7-element digital DQPSK DM system are now presented.

First of all, in order to verify the orthogonality between information and injected interference along the selected communication direction of 60°, the BER spatial distributions, obtained by both simulations that are based on the measured antenna array far-field radiation patterns and experiments, under SNR of 13 dB are depicted in Fig. 8. The SNR of 13 dB was selected since it returned reasonably low and stable, but not zero, BER value along 60°. We can see that the BER experiment and simulation results largely resemble each other. That there is little influence of the injected interference on the BER along the 60° direction indicates the required orthogonality. It is also observed that the injected interference has the capability of narrowing main BER beam as was presented in [10].

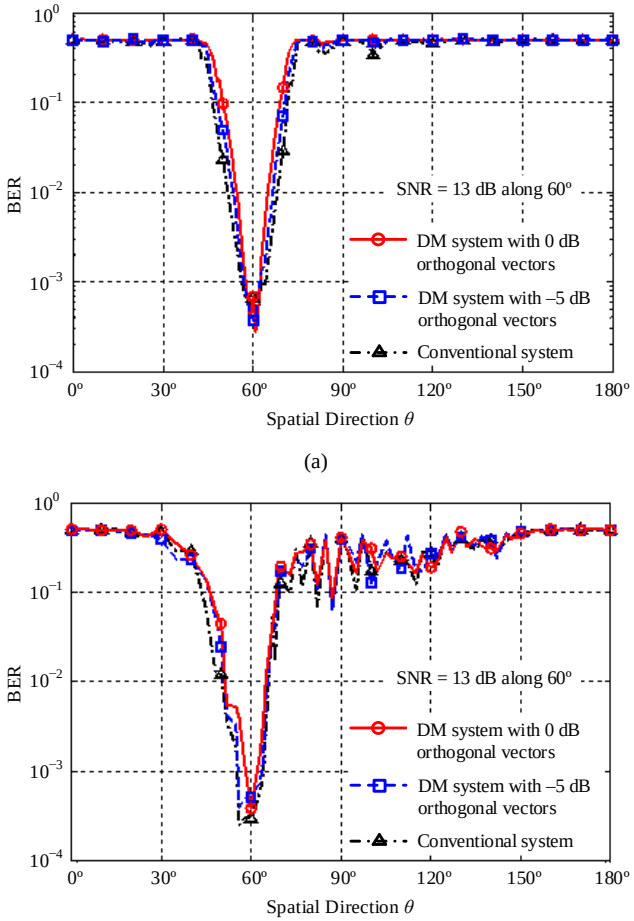

Fig. 8. (a) BER simulation results based on the measured antenna array far-field patterns and (b) BER experimental results of the 7-element digital DQPSK DM system. SNR along 60° is set to 13 dB.

Secondly, in order to illustrate the superiority of the DM systems on suppressing BER sidelobes over the conventional system, we repeated the same simulations and experiments but with SNR increased by 10 dB, see Fig. 9. When compared with the BER simulation results in Fig. 9 (a), the experimental results in Fig. 9 (b) show narrower BER main beams and more noticeable BER sidelobes. The narrower BER main beams obtained in the experiment may be caused by additional distortions imposed by transmit gain non-linearity and/or by imprecise recovery of the preamble sequence at receive sides. In simulations, none of these errors are considered [31]. The lower BER sidelobes, particularly along directions around boresight, may be the results of signals reflected by equipment placed in the anechoic chamber and/or the signals directly coupled onto the receive WARP node. It is noted that the equipment of AWG5012 and the receive WARP board were located around 60° in azimuth, where no interference was projected, in the anechoic chamber, see arrangement in Fig. 10. Despite these features, agreement between simulation and experiment is good.

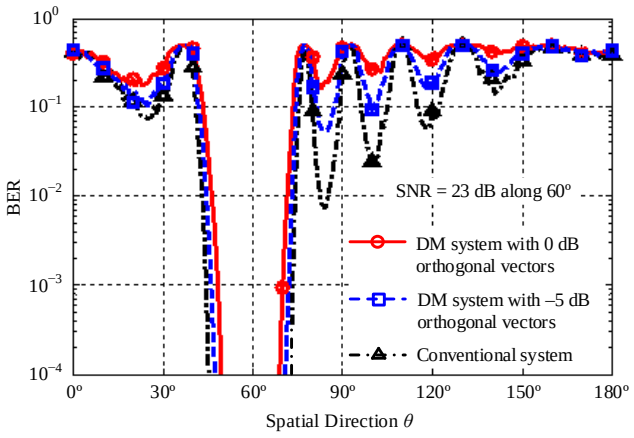

(a)

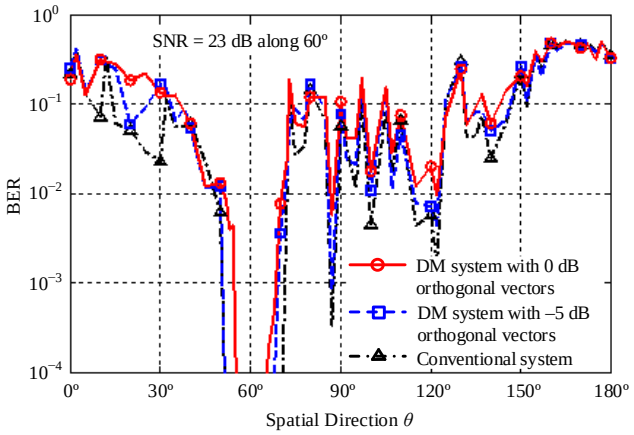

(b)

Fig. 9. (a) BER simulation results based on the measured antenna array patterns and (b) BER experiment results of the 7-element digital DQPSK DM system. SNR along 60° is set to 23 dB.

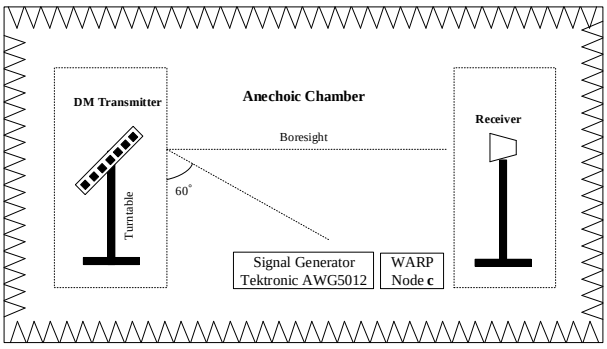

Fig. 10. Equipment arrangement for digital DM experiment.

VI. Conclusions

In this paper, a digital DQPSK DM system implementation and experimental results were presented. Several practical aspects, especially the system calibration, were discussed in detail. The BER experimental results well resemble the simulation results with slight explainable discrepancies. As were repeatedly presented for the DM synthesis approaches discussion in previous work, two advantages in terms of secrecy that DM systems possess over conventional systems, i.e., narrower BER main beams and higher BER values associated with BER sidelobes, could be observed in the experimental results. To the best of the authors' knowledge, it is the first dynamic DM demonstrator operating with real-time data transmissions that has ever been reported. The BER experimental results validated both the digital DM architecture and the applied orthogonal vector DM synthesis approach.

References

[1] A. Babakhani, D. B. Rutledge, and A. Hajimiri, "Transmitter architectures based on near-field direct antenna modulation," *IEEE J. Solid-State Circuits*, Vol. 43, No. 12, 2674–2692, Dec. 2008.

[2] A. Babakhani, D. Rutledge, and A. Hajimiri, "Near-field direct antenna modulation," *IEEE Microw. Mag.*, Vol. 10, No. 1, 36–46, Feb. 2009.

[3] A. H. Chang, A. Babakhani, and A. Hajimiri, "Near-field direct antenna modulation (NFDAM) transmitter at 2.4 GHz," IEEE Int. Symp., Antennas Propagat. Soc. (APSURSI '09), 2009, 1–4.

[4] M. P. Daly and J. T. Bernhard, "Directional modulation technique for phased arrays," *IEEE Trans. Antennas Propag.*, Vol. 57, No. 9, 2633–2640, Sep. 2009.

[5] M. P. Daly and J. T. Bernhard, "Beamsteering in pattern reconfigurable arrays using directional modulation," *IEEE Trans. Antennas Propag.*, Vol. 58, No. 7, 2259–2265, Jul. 2010.

[6] M. P. Daly, E. L. Daly, and J. T. Bernhard, "Demonstration of directional modulation using a phased array," *IEEE Trans. Antennas Propag.*, Vol. 58, No. 5, 1545–1550, May 2010.

[7] M. Bloch and J. Barros, Physical-Layer Security From Information Theory to Security Engineering. Cambridge, U.K.: Cambridge Univ. Press, 2011.

[8] S. William, Cryptography and Network Security. 4th ed. Pearson Education India, 2006.

[9] Y. Ding and V. Fusco, "Vector representation of directional modulation transmitters," 8th Eur. Conf. on Antennas Propag. (EUCAP), 2014, 332–336.

[10] Y. Ding and V. Fusco, "A vector approach for the analysis and synthesis of directional modulation transmitters," *IEEE Trans. Antennas Propag.*, Vol. 62, No. 1, 361–370, Jan. 2014.

[11] H. Shi and T. Alan, "Direction dependent antenna modulation using a two element array," 5th Eur. Conf. Antennas Propag. (EUCAP), 2011, 812–815.

[12] H. Shi and A. Tennant, "An experimental two element array configured for directional antenna modulation," 6th Eur. Conf. Antennas Propag. (EUCAP), 2012, 1624–1626.

[13] H. Shi and A. Tennant, "Secure communications based on directly modulated antenna arrays combined with multi-path," Antennas Propag. Conf. (LAPC), Loughborough, U.K., Nov. 11–12, 2013, 582–586.

[14] H. Shi and A. Tennant, "Enhancing the security of communication via directly modulated antenna arrays,"

IET Microw., Antennas Propag., Vol. 7, No. 8, 606–611, Jun. 2013.

[15] H. Shi and A. Tennant, "Simultaneous, multichannel, spatially directive data transmission using direct antenna modulation," *IEEE Trans. Antennas Propag.*, Vol. 62, No. 1, 403–410, Jan. 2014.

[16] Y. Ding and V. Fusco, "Directional modulation transmitter synthesis using particle swarm optimization," Antennas Propag. Conf. (LAPC), Loughborough, U.K., Nov. 11–12, 2013, 500–503.

[17] Y. Ding and V. Fusco, "BER driven synthesis for directional modulation secured wireless communication," *Int. J. Microw. Wireless Technol.*, Vol. 6, No. 2, 139–149, Apr. 2014.

[18] Y. Ding and V. Fusco, "Directional modulation transmitter radiation pattern considerations," *IET Microw., Antennas Propag.*, Vol. 7, No.15, 1201–1206, Dec. 2013.

[19] Y. Ding and V. Fusco, "Constraining directional modulation transmitter radiation patterns," *IET Microw., Antennas Propag.*, Vol. 8, No.15, 1408–1415, Dec. 2014.

[20] T. Hong, M. Z. Song, and Y. Liu, "RF directional modulation technique using a switched antenna array for physical layer secure communication applications," *Progress in Electromagn. Res.*, Vol. 116, 363–379, 2011.

[21] N. Valliappan, A. Lozano, and R. W. Heath, "Antenna subset modulation for secure millimeter-wave wireless communication," *IEEE Trans. Commun.*, Vol. 61, No. 8, 3231–3245, Aug. 2013.

[22] Q. Zhu, S. Yang, R. Yao, and Z. Nie, "A directional modulation technique for secure communication based on 4D antenna arrays," 7th Eur. Conf. on Antennas and Propag. (EUCAP), 2013, 125–127.

[23] Q. Zhu, S. Yang, R. Yao, and Z. Nie, "Directional modulation based on 4-D antenna arrays," *IEEE Trans. Antennas Propag.*, Vol. 62, No. 2, 621–628, 2014.

[24] Y. Ding and V. Fusco, "Sidelobe manipulation using Butler matrix for 60 GHz physical layer secure wireless communication," Antennas Propag. Conf. (LAPC), Loughborough, U.K., Nov. 11–12, 2013, 61–65.

[25] Y. Zhang, Y. Ding, and V. Fusco, "Sidelobe modulation scrambling transmitter using Fourier Rotman lens," *IEEE Trans. Antennas Propag.*, Vol. 61, No. 7, 3900–3904, Jul. 2013.

[26] "WARP project." [Online]. Available: http://www.warpproject.org. [Accessed: 14-Jun-2014].

[27] "Maxim Integrated, MAX2828/MAX2829 datasheet." [Online]. Available: http://www.maximintegrated.com. [Accessed: 14-Jun-2014].

[28] "Gil Technologies, GML 1000 high frequency laminate." [Online]. Available: http://www.apcircuits.com/resources/information/gml10060. pdf. [Accessed: 14-Jun-2014].

[29] D. M. Pozar, "The active element pattern," *IEEE Trans. Antennas Propagat.*, Vol. 42, 1176–1178, 1994.

[30] "Tektronix, AWG5000 series." [Online]. Available: http://www.tek. com. [Accessed: 14-Jun-2014].

[31] Y. Ding and V. Fusco, "Establishing metrics for assessing the performance of directional modulation systems," *IEEE Trans. Antennas Propag.*, Vol. 62, No. 5, 2745–2755, May 2014.

Yuan Ding received his Bachelor's degree from Beihang University (BUAA), Beijing, China, in 2004 and received his Master's degree from Tsinghua University, Beijing, China, in 2007, both in Electronic Engineering.

He was a RF engineer in Motorola R&D center (Beijing, China) from 2007 to 2009, before joining Freescale semiconductor Inc. (Beijing, China) as a RF field application engineer, responsible for high power base-station amplifier design, from 2009 to 2011. He is currently working toward his Ph.D. degree at the ECIT institute, Queen's University of Belfast, Belfast, United Kingdom. His research interests are in antenna array and physical layer security. He was the recipient of the IET Best Student Paper award at LAPC 2013. He was the recipient of the Young Scientists Awards in General Assembly and Scientific Symposium (GASS), 2014 XXXIst URSI.

Vincent F. Fusco received the Bachelor's degree (1st class honors) in electrical and electronic engineering, the Ph.D. degree in microwave electronics, and the D.Sc. degree, for his work on advanced front end architectures with enhanced functionality, from The Queens University of Belfast (QUB), Belfast, Northern Ireland, in 1979, 1982, and 2000, respectively.

He holds a personal chair in High Frequency Electronic Engineering at Queens University of Belfast (QUB). His research interests include active antenna and front-end MMIC techniques. He is head of the High Frequency Laboratories at QUB where he is also director of the International Centre for System on Chip for Advanced Microwireless. Professor Fusco has published over 450 scientific papers in major journals and in referred international conferences. He has authored two textbooks, holds patents related to self-tracking antennas and has contributed invited papers and book chapters.

Prof. Fusco serves on the technical program committee for various international conferences including the European Microwave Conference. He is a Fellow of both the Institution of Engineering and Technology and the Institute of Electrical and Electronic Engineers. In addition he is a Fellow of the Royal Academy of Engineers and a member of the Royal Irish Academy. In 2012 he was awarded the IET Senior Achievement Award the Mountbatten Medal.